EFFECT OF LARGE-SCALE MAGNETIC FIELDS ON TOTAL SOLAR IRRADIANCE

A. V. MORDVINOV[1] and R. C. WILLSON[2]
[1]*Institute of Solar-Terrestrial Physics, P.O. Box 4026, Irkutsk, 664033, Russia*
(e-mail: avm@iszf.irk.ru)
[2]*Center for Climate Systems Research, Columbia University, Coronado, California, U.S.A.*
(e-mail: acrim@acrim.com)

(Received 20 September 2002; accepted 8 March 2003)

Abstract. The effect of large-scale magnetic fields on total solar irradiance (TSI) was studied both in time–frequency and in time–longitude aspects. A continuous wavelet analysis revealed that the energy of thermomagnetic disturbances due to sunspots and faculae cascades into the magnetic network and facular macrostructure. A numerical technique of time–longitude analysis was developed to study the fine structure of temporal changes in the TSI caused by longitudinal brightness inhomogeneities and rotation of the Sun. The analysis facilitates mapping large-scale thermal inhomogeneities of the Sun and reveals patterns of radiative excesses and deficits relative to the undisturbed solar photosphere. These patterns are organized into 2- and 4-sector structures that exhibit the effects of both activity complexes and magnetically active longitudes. Large-scale patterns with radiative excess display a facular macrostructure and bright patterns in the magnetic network caused by the dissipation of large-scale thermomagnetic disturbances. Similar global-scale temperature patterns were found in the upper solar atmosphere. These temperature patterns are also causally related to long-lived magnetic fields of the Sun. During activity cycles 21 – 23 the patterns with radiative excess tend to be concentrated around the active longitudes which are centered at about 60° and 230° in the Carrington system.

1. Introduction

Continuous monitoring of the Sun by satellite experiments during the past two decades, complemented by earlier observations and ground-based measurements of solar indices, have clearly shown that basic physical parameters of the Sun are time dependent. It has been discovered that the solar properties of luminosity, solar rotation, and magnetic fields vary over the solar magnetic activity cycle (Willson and Hudson, 1991; Howard and LaBonte, 1980; Livingston *et al.*, 1991). These global changes are inter-related in a complex way and signify that large-scale thermomagnetic disturbances occur in the convective zone of the Sun over a wide range of time scales (Pap *et al.*, 2001).

The magnetohydrodynamic dynamo driven by solar convection and rotation generates magnetic fields which, in a feedback manner affect the heat transport and rotation, thereby inducing large-scale thermomagnetic disturbances within the convection zone (Rüdiger and Kitchatinov, 1990; Spruit, 1991; Pipin and Kitchatinov,

Solar Physics **215:** 5–16, 2003.

2000). Both the deep-seated and surface thermomagnetic disturbances dissipate into heat and radiation in the solar atmosphere on a wide range of timescales (Endal, Sofia, and Twig, 1985). As an 11-yr cycle progresses solar luminosity varies by an amount of about 0.1% in amplitude (Willson and Hudson, 1991). The photospheric impact of magnetic activity in the form of sunspots, faculae and the magnetic network modulate solar luminosity (Willson *et al.*, 1981; Foukal and Lean, 1988). In addition to these well-known phenomena related to concentrated magnetic flux tubes, large-scale magnetic fields may also contribute to TSI variability.

The magnetic fields of the Sun demonstrate multi-scale and hierarchical structures. Sunspots are clustered on time and spatial scales of sunspot groups and activity complexes. Moreover, strong active phenomena are concentrated in global patterns known as the magnetically active longitudes (Bumba and Howard, 1969). Long-lived longitudinal patterns persist for many years and keep their identity from one activity cycle to the next (Vitinsky, Kopecký, and Kuklin, 1986; Bumba and Hejna, 1991). These large-scale magnetic patterns are characterized by a quasi-rigid rotation that often differs from the Carrington rotation rate. The organization and evolution of large-scale magnetic activity derived from different indices differ in detail, but common features have been inferred from previous studies (Bumba and Hejna, 1991). The active longitudes are often localized near 180° apart, thereby inducing an approximately 13.5-day periodicity in temporal changes of solar indices (Donnelly and Puga, 1990; Pap *et al.*, 2001).

In this paper we studied the influence of large-scale activity organization on total solar irradiance (TSI) variability both in time–frequency and in time–longitude aspects. We found global-scale patterns of radiative excess and deficit relative to the undisturbed solar photosphere caused by long-lived magnetic structures such as activity complexes and magnetically active longitudes. The most stable patterns are associated with persistent active longitudes and may manifest the non-axisymmetric relic magnetic field of the Sun that was captured at the early stages of its evolution (Kitchatinov, Jardine, and Cameron, 2001). Long-term changes in the large-scale magnetic fields of the Sun (Lockwood, Stamper, and Wild, 1999) can also produce TSI variations on a secular time scale (Willson, 1997).

2. Time–Frequency TSI Variability

Total solar irradiance has been monitored since 1978 by a series of space flight experiments: Nimbus-7/ERB (Hickey *et al.*, 1980; Hoyt and Kyle, 1990), SMM/ACRIM-I (Willson and Hudson, 1991), ERBS (Lee *et al.*, 1995), UARS/ACRIM-II (Willson, 1997), SOHO/VIRGO (Fröhlich and Lean, 1998), and ACRIMSAT/ACRIM-III (Willson, 2002). Based on these long-term, high-precision TSI measurements, various composite models of the TSI time series have been constructed using different approaches and assumptions (Fröhlich and Lean, 1998; Willson,

TABLE I
Space experiments used in construction of the ACRIM TSI composite.

Experiment	Lifetime	Results in time series	Time series fraction
Nimbus7/ERB	1978 – 1993	1978 – 1980	0.054
		1984 (ACRIM1 gap)	0.007
		1989 – 1991	0.097
		1992 (ACRIM2 gap)	0.006
SMM/ACRIM1	1980 – 1989	1980 – 1989	0.404
UARS/ACRIM2	1991 →	1991 – 1996	0.366
		1998 – 2000	
SOHO/VIRGO	1996 →	1996 – 1998	0.110
ACRIMSAT/ACRIM3	2000 →	2000 →	0.066
Total Nimbus7/ERB	1978 – 1993	1978 – 1992	0.165
Total ACRIM	1980 – 2001	1980 – 2001	0.725
Total SOHO/VIRGO	1996 →	1996 – 1998	0.110

2002; Willson and Mordvinov, 2003). Despite some minor differences they are equivalent for the purposes of this study (Willson and Mordvinov, 1999). The ACRIM TSI composite time series uses Nimbus7/ERB, ACRIM1, 2 & 3 and VIRGO results normalized to the ACRIM3 scale using overlapping comparisons. The relationship of ACRIM1 and ACRIM2 results are derived from NIMBUS7/ERB comparisons. A new version of the composite TSI time series (Willson and Mordvinov, 2003) is based on the most recent results from satellite observations described in Table I. A time series of TSI daily means is plotted in Figure 1(a).

Continuous wavelet analysis (Vigouroux, Pap, and Delache, 1997; Crommelynk and Dewitte, 1997; Willson and Mordvinov, 1999) revealed non-stationary time-frequency TSI behavior over solar activity cycles. Figure 1(b) shows the power wavelet spectrum for a new version of the TSI composite. Estimated using the Morlet wavelet function, the power spectrum displays the complex energetics of the TSI signal.

The energy of thermomagnetic disturbances caused by sunspots and faculae concentrates at the rotational timescale of about 27 days. These recurring events appear at multiple timescales of about 54 and 81 days in the wavelet spectrum, corresponding to their 2nd and 3rd reappearances. In cycle 22 these thermomagnetic disturbances due to sunspots and faculae strengthened during both the first and secondary maxima of solar activity.

Significant annual periodicity persists throughout the TSI record even after all the measurements are adjusted to 1 AU. This seems to be due to the Earth's orbital motion. Annual periodicity is also observed in the interplanetary magnetic field

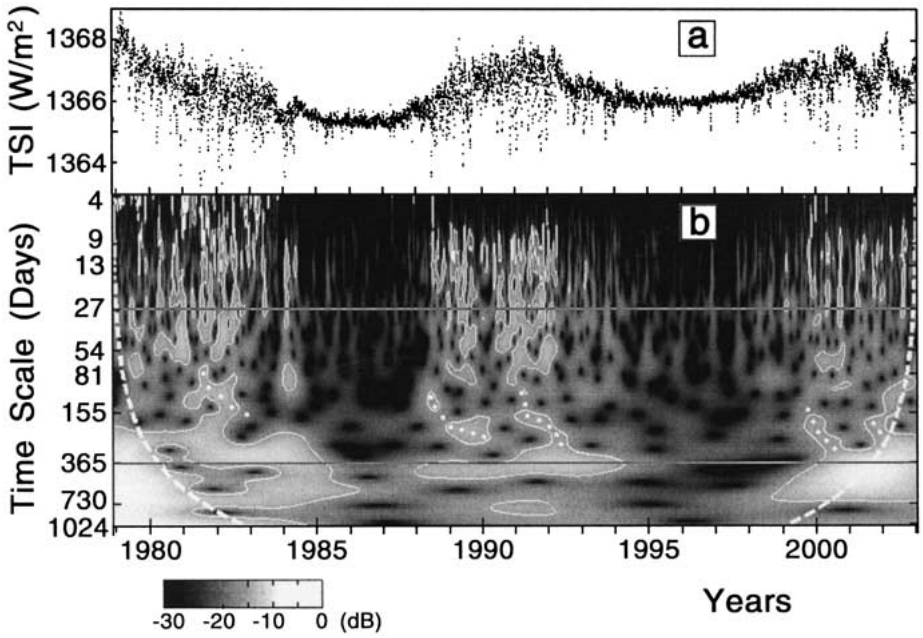

Figure 1. The composite TSI time series (a), and its power wavelet spectrum (b). The spectrum is normalized to its maximum value and it is plotted in a decibel scale. The limit of useful results is shown by the *white dashes. White contour lines* indicate 0.8 significance level. *Dots* trace the energy cascades.

(Rosenberg and Coleman, 1969) and in the solar mean magnetic field (SMMF) signal (Kotov, Levitsky, and Stepanyan, 1981). Similarity between TSI and SMMF signals will be discussed below. It is reasonable to suppose a universal annual modulation of full-disk solar parameters. So, in addition to intrinsic TSI variability a subtle signal is generated by the annual movement of the Earth in its orbit whose plane is inclined to the ecliptic by 7.25 deg. The Earth's excursions relative to the ecliptic plane provide a maximum view of the Sun's northern hemisphere in September and southern in March. This provides an annual signal near 365 days, caused by asymmetries in the solar activity of the two solar hemispheres. When solar activity is at a minimum no evidence of this signal exists. The influence of an inclined rotation axis of the Sun on TSI variations appears also on a wide time scale range due to this geometrical reason (Knaack *et al.*, 2001).

The phase wavelet spectrum characterizes the signal's phase behavior and displays the synergetics of its components regardless of their energy contents. The TSI composite and its phase wavelet spectrum are shown in Figures 2(a) and 2(b), respectively. A horizontal cross-section of this spectrum describes phase changes for a given timescale. For example, a cross-section at the 365-day timescale characterizes the phase of the annual TSI variation. Change in color from black to white corresponds to the phase of the annual TSI variation from -180 to $+180$ deg. The

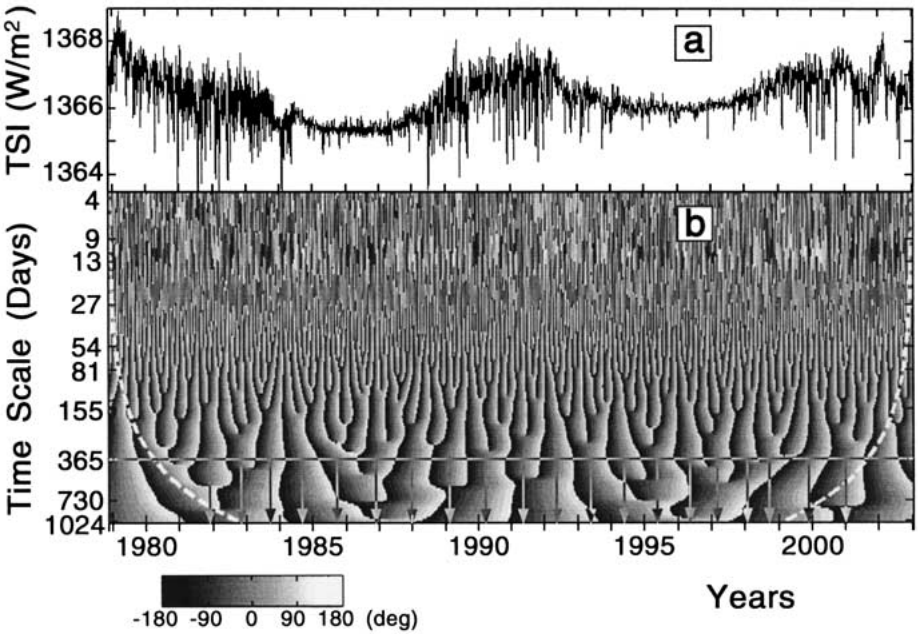

Figure 2. The TSI composite (a), and its phase wavelet spectrum (b). *Dashes* indicate the edge distortions.

phase behavior is not synchronized within a year because of superposition of the annual variation with intrinsic TSI variability. As a result the annual TSI variation peaks at different days of year as indicated by the arrows in Figure (2b).

A continuous wavelet analysis (Willson and Mordvinov, 1999) revealed that the energy of thermomagnetic disturbances cascades to longer timescales through the 155-day timescale during the first and secondary maxima of activity cycle 22. In the current cycle a similar energetic cascade occurred in 1999–2000. In 2001–2002 we see a complicated structure on the intermediate timescales. This resulted from superposition of the second energetic cascade with an increase in activity-brightness in 2001. Besides, at significance level 0.8 the edge error is not negligible near the ends of the TSI record. So, these two different patterns merged and produce a complicated structure. As the current cycle progresses, these details will be resolved better. In Figure 1(b) these cascades are marked with white dots within the features of which significance level exceeds 0.8 according the statistical test by Torrence and Compo (1998).

The 155-day periodicity appears in many solar indices related to flare ensemble, faculae, X-ray flux, etc. (Bai, 1988; Lean, 1990). All these phenomena dissipate the magnetic energy in a global sense and tend to cluster in large-scale patterns ('hot spots', facular macrostructure, active longitudes). Cascading to longer spatial and temporal timescales the energy resembles a relaxation that appears in TSI and radiant indices. This suggests that the 155-day periodicity originates after the re-

laxation of thermomagnetic disturbances which supply energy both in the magnetic network and in facular macrostructure (Willson and Mordvinov, 1999).

3. Wavelet-Deconvolution of the Composite TSI Time Series

The observed TSI is a convolution of the brightness distribution over the solar disk with the limb darkening function. Although TSI is a full-disk solar index, the rotation of the Sun makes it possible to extract information about the spatial distribution of persistent brightness inhomogeneities. A comparison of TSI values from rotation to rotation (e.g., in the Bartels format) enables us to recover, roughly, these brightness inhomogeneities as a function of heliographic longitude. Analogously, there is a possibility to recover precisely a long-lived brightness distribution over the heliographic longitude using a numerical deconvolution that carries out an inversion of a sequence of the TSI values. Based on analysis of the fine structure in TSI signal, a new technique was developed (Mordvinov and Willson, 2001) that enables us to map the longitudinal brightness distribution.

The central idea behind the wavelet deconvolution technique is to filter out the rotational modulation from the TSI signal and to plot this component, rotation by rotation, as a time–longitude diagram. A similar diagram plotted for the SMMF revealed a multi-mode regime of solar rotation and its cyclic behavior (Mordvinov and Plyusnina, 2000, 2001).

The orthogonal wavelet transform can be used as a powerful filtering tool. In this study we used the orthogonal Daubechies wavelets as analyzing functions. The discrete wavelet decomposition of TSI as a time dependent function on a dyadic time scale may be written as

$$\mathrm{TSI}(t) = \sum_{j,k=-\infty}^{\infty} c_{jk}\psi_{jk}(t), \tag{1}$$

where ψ_{jk} are the Daubechies wavelets, and the wavelet-coefficients determined as the inner products $c_{jk} = \langle TSI \cdot \psi_{jk}\rangle$ (Daubechies, 1992).

The essential effects of rotational modulation fall within the range of timescales of 13–30 days. Therefore, when computing the inverse wavelet transform we keep the coefficients which correspond to 8, 16, 32 day timescales. Hence, the filtered component that contains essential rotational effects has the form

$$\delta\mathrm{TSI}(t) = \sum_{j=3}^{5} \sum_{k=-\infty}^{\infty} c_{jk}\psi_{jk}(t), \tag{2}$$

with index j referred to the rotational timescales of 2^j days, where $j = 3, 4, 5$. Figures 3(a) and 3(b) show the TSI composite and the filtered out component or rotational modulation of TSI, respectively.

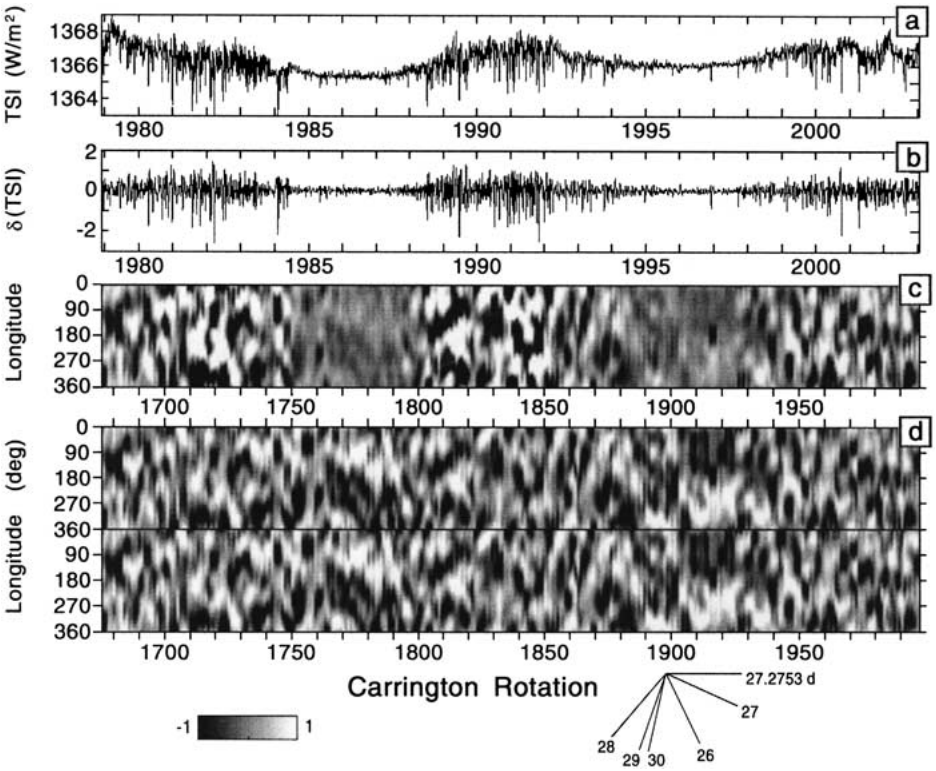

Figure 3. The TSI composite (a), and the 'rotational' component δ(TSI) (b); time–longitude diagram of δ(TSI) (c); time–longitude diagram of δ(TSI) normalized to the maximum value within each Carrington rotation (d). The ranges for the bar should be multiplied by factor 0.75 W/m^{-2} for panel (c). The *inclined lines* at the bottom indicate corresponding periods in days.

Then we plot the filtered out component as a time–longitude diagram with Carrington period folding. Using spline interpolation, we rearrange the filtered component in segments of Carrington period duration 27.2753 days and plot these segments, rotation by rotation, as vertical scans in the diagram shown in Figure 3(c). The vertical extent of each Carrington rotation corresponds to the heliographic longitude. There are global-scale coherent patterns in the time–longitude brightness distribution, seemingly related to long-lived magnetic fields. TSI variations corresponding to radiative excesses are shown in light halftones. Those corresponding to radiative deficits are shown in dark halftones. What can be seen in this figure are large thermal patterns of the solar photosphere itself with large-scale patterns of both excess (light) and deficit (dark) radiation against the nominal background radiation (50% gray).

4. Large-Scale Thermomagnetic Structures in the Photosphere and Corona

Figure 3(c) shows the smoothed time–longitude distribution of TSI variations. The diagram reveals large-scale organization in TSI deviations due to activity complexes, facular macrostructure, and the active longitudes. In the diagram we can see large-scale brightness disturbances on timescales of activity complexes with a characteristic duration from 0.5 to 1 yr. Vast regions of excess radiation caused by facular macrostructure can be seen during the two solar minima 1985–1987 and 1995–1997. These hotter features dominate during epochs of minimum activity when only few sunspots, at most, appear on the Sun.

The alternating hotter and cooler patterns in the vertical cross-section of the diagram correspond to two- and four-sector distributions of thermal disturbances and resemble sector magnetic fields. Sector patterns in brightness distribution alternate with each other and evolve during activity cycles 21–23. The four-sector brightness distribution generates a 13.5-day periodicity in TSI. In early 1984 there were two large TSI dips that exhibited a strong 4-sector structure in the time-longitude diagram, and a synchronously significant 13-day periodicity appears in the TSI wavelet spectrum (Willson and Mordvinov, 1999).

The first and secondary activity peaks in cycle 22 demonstrated cascades of spectral energy or 'relaxation tails' in the wavelet spectrum (Willson and Mordvinov, 1999). They both correspond to four-sector structures in the time–longitude diagram, suggesting that the cascades take place synchronously with a 4-sector thermomagnetic structure involving large-scale cells.

Estimation of the rotation rate of these patterns does not depend on the amplitude of the TSI variations so we can normalize each Carrington rotation to its maximum value without a loss of information. Figure 3(d) displays twice the normalized TSI diagram and illustrates clearly the effects of rotation regardless of a level of solar activity or a phase of the 11-yr cycle.

By analogy with a stroboscope in the time–longitude diagram the patterns aligned in a horizontal direction exhibit the Carrington rotation rate. The linearly inclined patterns indicate rigid rotation modes in the diagram. Similar coherent patterns related to large-scale magnetic fields demonstrate their rigid rotation with synodic periods 27–31 days (Mordvinov and Plyusnina, 2000). Fast-rotating structures shift from rotation to rotation in a westward direction in the Carrington system and appear as backslash-inclined patterns. Modes of slow rotation appear at the diagram as slash-inclined patterns. The relation between the inclinations and the periods of rotation is shown at the bottom of Figure 3.

In the beginning of cycle 22 from mid-1988 to late 1989 the inclined features related to TSI deficit yield synodic periods of about 27.8 and 26.4 days, indicating that they were caused by activity complexes. During the minima epochs for 1985–1987 and 1995–1996, large regions of facular macrostructure and their corresponding radiative excess dominate. These exhibit faster rotation rates with periods of 26.1, 26.6, and 26.8 days.

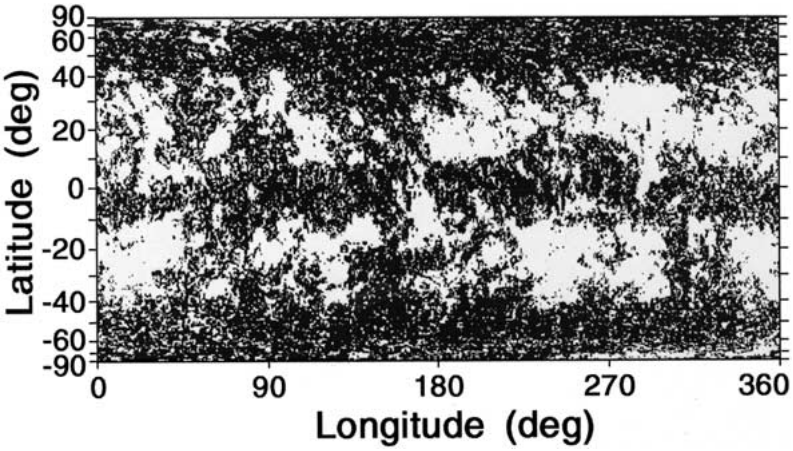

Figure 4. The summary distribution of ultraviolet radiation in the He II 304 Å line exceeding the threshold is accumulated for 1907 – 1962 Carrington rotations.

In the solar corona, global-scale patterns appear also if we plot a summary distribution of excess ultraviolet emission as a function of heliographic longitude using the Carrington maps of irradiance. The results, for the He II 304 Å line shown in Figure 4 are derived from the SOHO Extreme-ultraviolet Imaging Telescope (EIT) and display solar EUV irradiance exceeding a threshold of 0.9 of its maximum value (Delaboudinière *et al.*, 2001). Aggregated EUV brightenings are seen to outline large-scale magnetic structures, well-defined patterns spanning about 60° in longitude, related to activity complexes. Similar patterns have been observed in the Fe XII (195 Å) line images by Veselovsky *et al.* (2001). As the Sun rotates these global-scale structures cause apparent TSI variations on rotational timescale.

Strong evidence for similar global scale temperature patterns in the upper solar atmosphere can be seen in the superposition of synoptic maps of ultraviolet radiation. In the corona and transition region of the Sun there are large-scale patterns related to stable magnetic structures at the photospheric level. Interconnected loops of activity complexes radiate X-rays and extreme ultraviolet (Moses *et al.*, 1997).

5. Relation between TSI Variability and Solar Mean Magnetic Field

Solar mean magnetic field (SMMF) is a fundamental physical parameter that characterizes the net contribution of solar magnetic fields. In previous studies analysis of the SMMF was carried out both in timescale and in time–longitude aspects (Mordvinov and Plyusnina, 2000, 2001). There are more regular patterns in the SMMF time–longitude diagram as compared with that for the TSI. At the phase of ascending activity SMMF patterns display slow-rotation modes with periods about of 28 days. At the phase of descending activity the 27-day rotation mode dom-

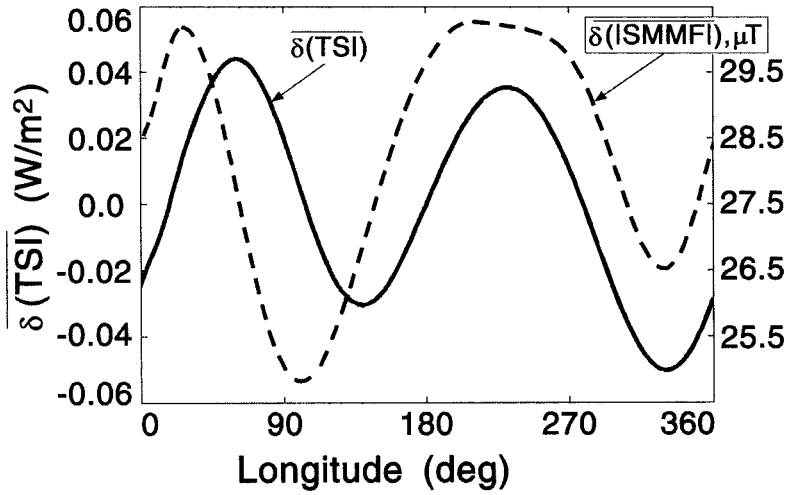

Figure 5. The longitudinal distribution of δ(TSI) (*solid*) and δ(|SMMF|) (*dashed*) averaged over the entire records.

inates. The 29–30-day periodicities appear episodically in the SMMF diagram. Similar rotation modes can also be traced in Figure 3(d).

It is also of interest to compare the average brightness distribution with large-scale magnetic fields over heliographic longitude. The average distribution of TSI deviations is estimated from the time–longitude diagram through averaging this over the entire record. A similar average distribution of the modulus δ(|SMMF|) was derived using the time–longitude diagram of time series obtained at Wilcox Solar Observatory over the period 1976–2002. The average distributions of both δ(TSI) and δ(|SMMF|) are shown in Figure 5. The bimodal δ(TSI) curve in Figure 5 represents the average longitudinal dependence of TSI deviation between 1978 and 2002. There are two well-defined active sectors on the Sun, at Carrington longitudes 60° and 230°, each characterized by long-term excess radiation. The distribution of large-scale magnetic fields is also non-uniform and related to the active longitudes (Benevolenskaya, Kosovichev, and Scherrer, 1999). Despite some shift both curves correlate well, demonstrating similar longitudinal dependencies and their causal relationship.

6. Conclusions

Time–frequency analysis of the composite TSI time series reveals its multi-scale and non-stationary behavior. Thermomagnetic disturbances due to sunspots, faculae, and activity complexes appear on the rotational timescales and its multiples. As these disturbances dissipate, their energy cascades to longer timescales. Characteristic inclined patterns are well-defined in cycles 21–23 during activity maxima.

The wavelet-deconvolution technique facilitates study of the longitudinal brightness disturbances of the Sun based on the analysis of the fine structure of the TSI time series. Large-scale temperature patterns related to long-lived magnetic structures appear in time–longitude diagrams of TSI variations. These thermal patterns are related to activity complexes, facular macrostructure and the magnetic network brightening. Huge hotter and cooler thermal patterns at the Sun are organized in two- and four-sector structures related to magnetic activity and display longitudinal patterns over an 11-yr cycle. Large-scale thermal disturbances alternate with each other and evolve during activity cycles 21–23. Global-scale temperature patterns are also manifested in an excessive EUV radiation from the upper solar atmosphere. Some thermal patterns exhibit modes of rigid rotation.

A comparative analysis of radiative and magnetic indices reveals their causal relationship and long-lived thermomagnetic disturbances at the Sun. Patterns with excessive radiation dominate and tend to concentrate at longitudes 60° and 230° which are located within or close to the 'superactive magnetic longitudes'. This reveals global scale temperature patterns related to the magnetically active longitudes over cycles 21–23. There are two well-defined sectors on the Sun which are characterized by an excess radiation in an averaged sense. Large-scale magnetic field, and magnetically active longitudes cause long-lived temperature patterns at the Sun and cause an anisotropy of solar radiation on long-term timescale.

Acknowledgements

The synoptic maps of EUV radiation and SMMF time series were taken from the EIT/SOHO and WSO websites by courtesy Drs E. E. Benevolenskaya, J. P. Delaboudinière, P. H. Scherrer, and J. T. Hoeksema. SOHO is a mission jointly operated by ESA/NASA. Work at the Institute of Solar-Terrestrial Physics was supported by the RFBR project 02-02-16044, and by the INTAS project 2001-0550. The National Aeronautics and Space Administration provides support for Dr Willson at Columbia University under contract NAS5-97164.

References

Bai, T.: 1988, *Astrophys. J.* **328**, 860.
Benevolenskaya, E. E., Kosovichev, A. G., and Scherrer, P. H.: 1999, *Solar Phys.* **190**, 145.
Bumba, V. and Hejna, L.: 1991, *Bull. Astron. Inst. Czech.* **42**, 76.
Bumba, V. and Howard, R.: 1969, *Solar Phys.* **7**, 28.
Crommelynk, D. and Dewitte, S.: 1997, *Solar Phys.* **173**, 177.
Daubechies, I.: 1992, *Ten Lectures on Wavelets*, Society for Industrial and Applied Mathematics, Philadelphia.
Delaboudinière, J. P. *et al.*: 2001, http://lasco-www.nrl.navy.mil/carr-maps/eit/.
Donnelly, R. F. and Puga, L. C.: 1990, *Solar Phys.* **130**, 369.
Endal, A. S., Sofia, S., and Twigg, L. W.: 1985, *Astrophys. J.* **290**, 748.

Foukal, P. V. and Lean, J.: 1988, *Astrophys. J.* **328**, 347.
Fröhlich, C. and Lean, J.: 1998, *Geophys. Res. Lett.* **25**, 4377.
Hickey, J. R., Stowe, L. L., Jacobowitz, H., Pellegrino, P., Maschoff, R. H., House, F., and Vonder Haar, T. H.: 1980, *Science* **208**, 281.
Hoyt, D. and Kyle, L.: 1990, in *Proc. Climate Impact of Solar Variability*, NASA Conf. Rep. 3086, NASA, Greenbelt, p. 293.
Howard, R. and LaBonte, B. J.: 1980, *Astrophys. J.* **239**, L33.
Kitchatinov, L. L., Jardine, M., Cameron, A. C.: 2001, *Astron. Astrophys.* **374**, 250.
Knaack, R., Fligge, M., Solanki, S. K., and Unruh, Y. C.: 2001, *Astron. Astrophys.* **376**, 1080.
Kotov, V. A., Levitsky, L. S., and Stepanyan, N. N.: 1981, *Izv. Krymsk. Astrofiz. Obs.* **63**, 3.
Lean J.: 1990, *Astrophys. J.* **363**, 718.
Lee III, R. B., Gibson, M. A., Willson, R. C., and Thomas, S.: 1995, *J. Geophys. Res.* **100**, 1667.
Livingston, W. C., Donnelly, R. F., Grigoryev, V. M., Demidov, M. L., Lean, J., Steffen, M., White, O. R., and Willson, R. C.: 1991, in A. N. Cox, W. C. Livingston, and M. C. Matthews (eds.), *Solar Interior and Atmosphere*, The University of Arizona Press, Tucson, p. 1109.
Lockwood, M., Stamper, R., and Wild, M. N.: 1999, *Nature* **399**, 437.
Mordvinov, A. V. and Plyusnina, L. A.: 2000, *Solar Phys.* **197**, 1.
Mordvinov, A. V. and Plyusnina, L. A.: 2001, *Astron. Reports* **45**, 753.
Mordvinov, A. V. and Willson, R. C.: 2001, *Astron. Letters* **27**, 528.
Moses, J. D., Clette, F., Delaboudinière, J. P. *et al.*: 1997, *Solar Phys.* **175**, 571.
Pap, J., Rozelot, J. P., Godier, S., and Varadi, F.: 2001, *Astron. Astrophys.* **372**, 1005.
Pipin, V. V. and Kitchatinov, L. L.: 2000, *Astron. Reports* **44**, 771.
Rosenberg, R. L. and Coleman, P. J.: 1969, *J. Geophys. Res.* **74**, 5611.
Rüdiger, G. and Kitchatinov, L. L.: 1990, *Astron. Astrophys.* **236**, 503.
Spruit, H. C.: 1991, in C. Sonett, M. Giapapa, and M. S. Matthews (eds.), *The Sun in Time*, University of Arizona Press, Tucson, p. 118.
Torrence, C. and Compo, G. P.: 1998, *Bull. Am. Meteorol. Soc.* **79**, 61.
Veselovsky, I. S., Zhukov, A. N., Dmitriev, A. V., Tarsina, M. V., Clette, F., Cugnon, P., and Hochedez, J. F.: 2001, *Solar Phys.* **201**, 27.
Vigouroux, A., Pap, J., and Delache, P.: 1997, *Solar Phys.* **176**, 1.
Vitinsky, Yu. I., Kopecký, M., and Kuklin, G. V.: 1986, *Statistics of Sunspot Activity of the Sun*, Nauka, Moscow, p. 314.
Willson, R. C.: 1997, *Science* **277**, 1963.
Willson, R. C.: 2002, http://www.acrim.com, http://acrim.jpl.nasa.gov
Willson, R. C. and Hudson, H. S.: 1991, *Nature* **351**, 42.
Willson, R. C. and Mordvinov, A. V.: 1999, *Geophys. Res. Lett.* **26**, 3613.
Willson, R. C. and Mordvinov, A. V.: 2003, *Geophys. Res. Lett.* **30**, 1199.
Willson, R. C., Gulkis, S., Janssen, M., Hudson, H. S., and Chapman, G. A.: 1981, *Science* **211**, 700.